Enhanced Magneto-Optical Activities of Modulated Fe-Pt Multilayer Metamaterials

Satoshi Tomita,[1,*,†,‡] Tomomi Suwa,[2] Patricia Riego,[3,4] Andreas Berger,[3] Nobuyoshi Hosoito,[1] and Hisao Yanagi[1]

[1] *Graduate School of Science and Technology, Nara Institute of Science and Technology, 8916-5 Takayama, Ikoma, Nara 630-0192, Japan*

[2] *Graduate School of Materials Science, Nara Institute of Science and Technology, 8916-5 Takayama, Ikoma, Nara 630-0192, Japan*

[3] *CIC nanoGUNE, E-20018 Donostia-San Sebastian, Spain*

[4] *Departamento de Física de la Materia Condensada, Universidad del País Vasco, UPV/EHU, E-48080 Bilbao, Spain*

We study optical and magneto-optical (MO) properties of epitaxially grown modulated Fe-Pt multilayer metamaterials by means of generalized MO ellipsometry (GME). Large Kerr rotation, ellipticity, and MO coupling parameters in the visible and near-infrared regions are obtained for modulated metamaterials, in which the stacking sequences follow an inverse Fibonacci series. In contrast, periodic multilayers show small MO parameters, although they otherwise exhibit magnetic and optical properties that are very similar to those for the modulated metamaterials. The present study demonstrates that specific thickness modulation can have a significant materials design potential for one-dimensional magnetic metamaterials.

I. INTRODUCTION

An emerging important issue in condensed matter physics and materials science is symmetry breaking [1,2]. Short-range translational symmetry is broken in quasiperiodic systems [3,4] and quasicrystals [5]. In particular, patterned materials on the nanoscale with specific modulations that are based on quasiperiodicity show intriguing phenomena [6–12]. A plasmonic structure consisting of the modulated metallic and dielectric multilayers, for which the stacking sequences follow a Fibonacci series, demonstrated experimentally an enhancement of light-matter interaction [13]. The stacking sequences in multilayers are also found to modulate interaction between plasmonic metallic layers [14]. Since the multilayers consist of thin layers much smaller than the wavelength of light, they can be referred to as multilayer metamaterials. These results observed in such plasmonic multilayer metamaterials motivate an investigation of magnetic counterparts, i.e., modulated magnetic multilayer metamaterials.

Periodic multilayers consisting of magnetic transition metals, for example, iron (Fe), separated by nonmagnetic metals, for example, platinum (Pt) [15–20], have attracted considerable interest, especially in the context of perpendicular magnetic recording media [21–25]. It is anticipated that broken short-range translational symmetry in magnetic multilayers leads to modulation in exchange coupling between magnetic layers, resulting in intriguing magnetic phenomena [26–29]. Indeed, modulated magnetic multilayer metamaterials were theoretically predicted to give rise to anomalous magnetic resistance [30] and ferromagnetic resonance [31], and were experimentally demonstrated to bring about quasi-isotropic magnetization [32]. Nevertheless, enhancement of light-matter interaction in such modulated magnetic multilayer metamaterials has yet to be explored experimentally. Because, in a magnetic system, the exchange coupling can be modulated on the nanometer length scale, precise control in layer thickness and stacking is indispensable. Therefore, in this paper, epitaxial-growth techniques in ultrahigh vacuum are utilized to prepare Fe multilayers separated by Pt spacers, whose thickness is represented by inverse Fibonacci numbers, that is to say, modulated Fe-Pt multilayer metamaterials.

In our work here, we study optical and magneto-optical (MO) properties of the modulated Fe-Pt multilayer metamaterials by means of ellipsometry, namely generalized

---

*tomita@tohoku.ac.jp

†Visiting scientist at CIC nanoGUNE, E-20018 Donostia-San Sebastian, Spain

‡Present address: Institute for Excellence in Higher Education, Department of Physics, Graduate School of Science, Tohoku University, Sendai, Miyagi 980-8578, Japan.

MO ellipsometry (GME) [33,34], at several wavelengths in the visible and near-infrared region. GME's main advantage is the ability to investigate complex MO parameters with unprecedented precision, since it allows one to determine optical and MO properties simultaneously [33–39]. In addition, the dispersion of the parameters can be obtained through spectroscopic GME measurements [40–42]. For our work, it is also relevant to notice that the light penetration depth in our material systems is lower than the thickness of the multilayer structure. In other words, seed layers, buffer layers, and substrates utilized in the epitaxial-growth technique do not contribute to the GME signal. In this way, we may observe enhanced light-matter interaction in the modulated magnetic metamaterials using surface-sensitive GME.

The present study highlights that, by introducing a modulation in the magnetic multilayer metamaterials, the MO coupling constant (Q) can be altered, while the refractive index (N) remains nearly unchanged. An important feature of metamaterials is the independent control of electromagnetic parameters, e.g., electric permittivity and magnetic permeability [43–48], resulting in interesting phenomena, for example, a negative index of refraction [49]. We demonstrate here the possibility of independent control of the MO parameters in magnetic multilayer metamaterials. Furthermore, the present work opens the door of magnetic metamaterials for possible applications, such as, for example, new metamaterials for magnetoplasmonic detection to be utilized in biosensing [50–53], which rely on optimized or generally enhanced MO coupling effects.

II. EXPERIMENTAL PROCEDURES

The multilayers are epitaxially grown on single-crystal MgO(100) substrates using an electron-beam evaporation technique in ultrahigh vacuum. Figures 1(a) and 1(b) show schematic sample structures. Gray and yellow colors correspond to Fe and Pt layers, respectively. We prepare two types of epitaxially grown Fe-Pt multilayers: a periodic multilayer (PM) [Fig. 1(a)] as a control structure and a modulated multilayer referred to as inverse Fibonacci multilayer (IFM) metamaterials [Fig. 1(b)]. In the following, the number next to the element symbol corresponds to film thickness in angstroms; for example, Fe10 represents a Fe layer with a thickness of 10 Å. In order to obtain epitaxially grown multilayers, an Fe10 seed layer followed by a Pt100 buffer layer is deposited on a single crystal MgO substrate.

The actual metamaterial structure comprises intercalated Fe and Pt layers. The Fe layer thickness is identical in both the PM and IFM samples, namely, 5 Å. As for the Pt, in the PM sample, the thickness of the Pt layer is constant at 20 Å [54,55]. The Fe5/Pt20 structure is repeated 13 times on top of the buffer layer, and the PM sample is thus represented by the sequence MgO/seed Fe10/buffer
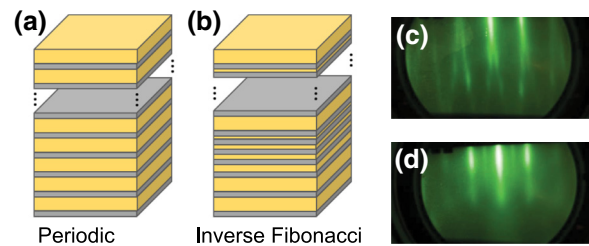

FIG. 1. Structures of Fe-Pt (a) periodic multilayer (PM) and (b) inverse Fibonacci multilayer (IFM) metamaterial. Gray and yellow colors correspond to Fe and Pt layers, respectively. *In situ* RHEED patterns of Pt(100) planes after the buffer Pt layer deposition (c) and after the IFM sample deposition (d).

Pt100/[Fe5/Pt20]$_{13}$. In contrast, in the IFM sample, the thickness of the Pt layers is not constant. Instead, its thickness gradually decreases following the Fibonacci number F_n, which can be written by a recursive formula given as $F_{n+2} = F_n + F_{n+1}$, where F_0 and F_1 correspond to 0 and 1, respectively. In this way, the nth Pt layer has a thickness corresponding to 20 Å divided by F_n from $n = 1$ to $n = 6$. The sequence is repeated twice in the sample and finally terminated by Fe5 and Pt20; namely, the IFM sample is represented by MgO/seed Fe10/buffer Pt100/[Fe5/Pt20/Fe5/Pt20/Fe5/Pt10/Fe5/Pt7/Fe5/Pt4/Fe5/Pt3]$_2$/Fe5/Pt20.

In GME measurements, a p-polarized light beam with an angle of incidence of 45° and wavelength λ ranging from 450 to 850 nm passes through a linear polarizer P_1 with its polarizing axis at an angle θ_1 from the s polarization. After being reflected on the sample surface, the light beam passes through a second linear polarizer P_2 with its polarizing axis at an angle θ_2 from the s polarization. The light intensity I after P_2 is detected by a photodiode. The sample is placed between the poles of an electromagnet that generates a magnetic field contained in the intersection between the plane of incidence of the light and the plane of the sample. As the sample magnetization $\pm M$ is consequently aligned in the in-plane direction and the applied field (± 1.2 kOe) is sufficient to saturate the samples (see Fig. 2), the longitudinal MO Kerr effect (LMOKE) configuration is achieved [see Fig. 3(a)].

III. RESULTS AND DISCUSSION

A. Multilayers characterization

The epitaxial growth of (100) planes of the seed Fe and buffer Pt layers on the substrate is confirmed by *in situ* reflection high-energy electron diffraction (RHEED). Figure 1(c) shows the RHEED pattern after the deposition of the Pt100 buffer layer. Streak lines in the RHEED pattern indicate that the Pt100 buffer layer is epitaxially grown on the Fe10 seed layer. Moreover, the split of the streak
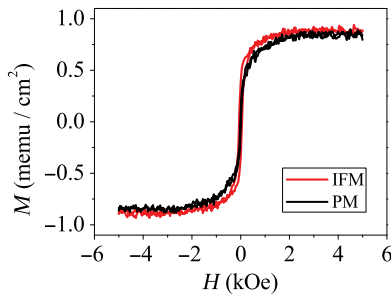
FIG. 2.   In-plane magnetic moment per sample area unit versus applied magnetic field measured by VSM. The IFM sample is shown as a red curve and the PM sample as a black curve.

lines at the bottom in the pattern is evidence of surface superstructures of the clean Pt surface, demonstrating the absence of intermixing between Pt and Fe.

Figure 1(d) shows the *in situ* RHEED pattern after deposition of the IFM sample. Similar to the RHEED pattern prior to the multilayer deposition in Fig. 1(c), streak lines in Fig. 1(d) highlight the epitaxial growth of the final capping Pt layer, indicating that the Fe and Pt layers are epitaxially grown throughout the multilayer. The streak lines shorten and have no splitting at the bottom, indicating that a small level of roughness is induced at the top Pt surface.

In-plane magnetization hysteresis loops are measured utilizing a MicroMag 3900 vibrating sample magnetometer (VSM). The results are shown in Fig. 2 for PM (black) and IFM (red) samples. As observed, given that both samples have the same Fe content (total Fe thickness of 75 Å, including 10 Å of the seed layer), their magnetic moment per sample area unit is the same. In addition, both have a similar reversal path, although the IFM sample saturates at slightly lower fields.

B. GME measurements

The GME measurements of the samples are carried out utilizing a wavelength-tunable laser to add spectroscopic capabilities to the GME setup used in Refs. [37,39]. The setup is sketched in Fig. 3(a). The key quantity to be measured in GME is the fractional change in light intensity $\delta I/I$ upon sample magnetization reversal ($\pm M$) [33,34],

$$\frac{\delta I}{I} = 2\frac{I(+M) - I(-M)}{I(+M) + I(-M)}, \qquad (1)$$

which is measured for various combinations of θ_1 and θ_2 illustrated in Fig. 3(a). Results of such measurements are shown in Figs. 3(b)–3(e) at four different wavelengths ($\lambda = 550$, 650, 750, and 850 nm) for the IFM sample. In Figs. 3(b)–3(e), the blue color corresponds to negative $\delta I/I$, while the red color corresponds to positive $\delta I/I$. Here, we can see that $\delta I/I(\theta_1, \theta_2)$ has two lobes of opposite sign that meet at the crossing point of the polarizers,
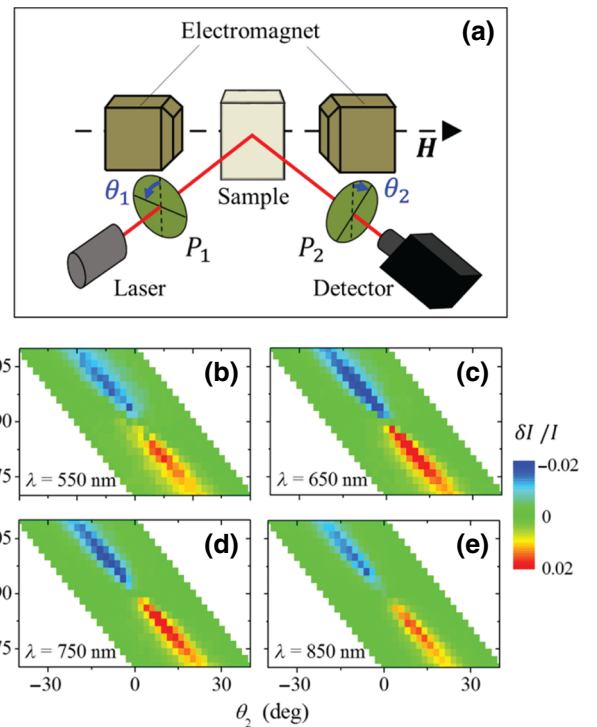

FIG. 3.   (a) Sketch of GME setup, showing the optical elements (laser, detector, and the two polarizers P_1 and P_2 with their respective angles θ_1 and θ_2) and sample implementation between the poles of the electromagnet. (b)–(e) $\delta I/I(\theta_1, \theta_2)$ maps, with an applied magnetic field of ± 1.2 kOe and for different λ: (b) $\lambda = 550$ nm, (c) $\lambda = 650$ nm, (d) $\lambda = 750$ nm, and (e) $\lambda = 850$ nm. The color scale for the four maps is shown to the right.

$\theta_1 = 90°$ and $\theta_2 = 0°$, which is a signature of LMOKE. We also observe that the maps are different for different λ, indicating the spectral sensitivity of the method.

We conduct $\delta I/I(\theta_1, \theta_2)$ measurements at several λ for both the PM and IFM samples. A fitting of each of the $\delta I/I(\theta_1, \theta_2)$ maps allows us to extract optical and MO variables of the sample [33,34]. Specifically, we can determine with a very high precision the Kerr rotation θ_K and ellipticity η_K values for each λ. The corresponding θ_K and η_K spectra are shown in Figs. 4(a) and 4(b), respectively. Error bars correspond to standard deviation in the fitting. As we can observe, both θ_K and η_K are far larger for the IFM sample, which is depicted in red squares, than for the PM sample, represented by black circles. In addition, the spectra of the IFM are strongly dependent on λ; we can even observe a sign change in θ_K at approximately $\lambda = 775$ nm. η_K remains negative in the explored wavelength region, but suffers a 40% decrease in absolute value from $\lambda = 550$ nm to $\lambda = 850$ nm. On the other hand, both θ_K and η_K for the PM sample appear nearly independent of λ and are about an order of magnitude smaller than those of the IFM sample.
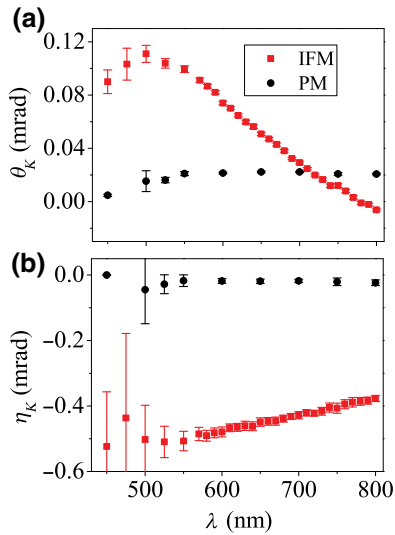
FIG. 4.   (a) θ_K and (b) η_K as a function of λ for PM (black circles) and IFM (red squares) samples.
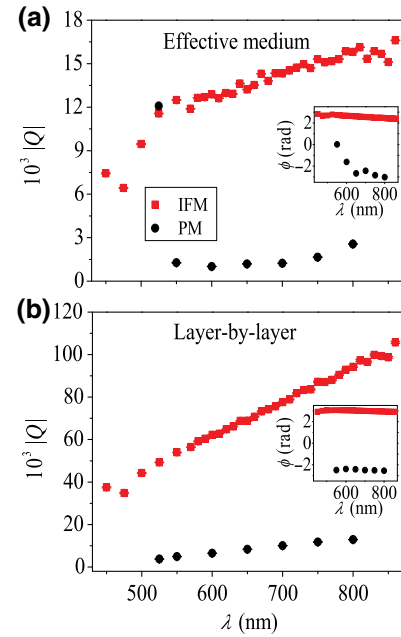

FIG. 5.   Spectral dependence of the amplitude of the MO coupling constant Q for samples IFM and PM, with an effective medium model (a) and a layer-by-layer optical model (b). Black circles and red squares correspond to PM and IFM samples, respectively. The insets show the phase ϕ of Q versus wavelength in each case.

C. Enhanced MO activity in modulated multilayer metamaterial

The experimentally measured optical and MO (θ_K and η_K) parameters allow us to determine the complex refractive index $N = n + i\kappa$ and the complex MO coupling parameter $Q = Q_r + iQ_i = |Q|e^{i\phi}$ of the material by fitting the data to an optical model. In the case of our samples, given that the thickness of the individual Fe and Pt layers is much smaller than the wavelength of the light utilized in our experiments, we perform an effective medium approximation, so that the optical properties of each sample are represented by an effective dielectric tensor with wavelength-dependent N and Q. In order to get N and Q for both samples, we calculate the optical and MO (θ_K and η_K) responses of the effective medium by means of a transfer matrix method [56] and we find the best-matching N and Q that fit the experimental data. For the model calculation, the incidence angle of light is set to 45°, as in our experiment, and the magnetization is taken to be aligned with the applied field, as the applied field magnitude is sufficient to saturate the magnetization in the GME experiment

Figure 5(a) shows the amplitude of the MO coupling $|Q|$ as a function of λ, for IFM (red squares) and for PM (black circles) in the effective medium approximation. $|Q|$ is about an order of magnitude larger in the IFM sample and has a clear wavelength dependence. The inset in Fig. 5(a) displays the phase ϕ of Q, which has an opposite sign between IFM and PM. We recall here that, for the IFM sample, θ_K in Fig. 4(a) changes the sign at approximately $\lambda = 775$ nm. In contrast, ϕ in the inset of Fig. 5(a) is almost constant, indicating that neither Q_r nor Q_i changes sign.

Therefore, the sign change in θ_K is traced back to an interplay between Q_r and Q_i, as well as between them and the optical constants. The real and imaginary part of the refractive index, n and κ, are found to be equal within the error bars for IFM and PM.

In the analysis above, we assume that the Fe-Pt multilayer metamaterials are effective media described by an effective N and Q. Given that PM and IFM samples contain identical volumes of Fe and show very similar in-plane magnetization curves in Fig. 2, the similar N (not shown here) that was fitted for PM and IFM samples verifies that the effective medium approximation is reasonable. We thus conclude that Fe-Pt IFM and PM samples have a similar N but very different Q as shown in Fig. 5(a), although they contain identical Fe volume. In other words, the effective Q of the modulated IFM sample is very much enhanced, if compared to the PM sample while retaining the same N.

D. Analysis with layer-by-layer model

A question that might arise is whether the different stacking of Fe and Pt can explain the enhanced Q in the IFM sample. Specifically, given that the IFM structure has more Fe close to the surface of the sample (because the Pt layers that are closest to the surface are thinner in IFM as compared to PM), one may argue that the enhanced Q of the medium is simply a consequence of this. However, this argument cannot explain such a massive enhancement

of Q in the IFM sample. The MOKE information depth, at which the signal for the Kerr rotation is reduced to $1/e$ of its surface value, is calculated for both samples and for several wavelengths over the studied spectral range and is found to be in the range of 12–15 nm. Additionally, we resort to a layer-by-layer optical model that includes all the individual layers in each of the samples, in such a way that each of the materials is described by its own wavelength-dependent dielectric tensor. The refractive indices N of Pt [57], Fe [58], and MgO [59] are fixed utilizing spectroscopic data reported in the literature. We then obtain the MO coupling Q of Fe (Pt is assumed to have $Q = 0$) by fitting the experimental data to the model.

The resulting $|Q|$ versus λ curves are shown in Fig. 5(b), in red squares for IFM and in black circles for PM. Also with this model, the amplitude of the MO coupling is much larger for the IFM sample, thus confirming that the sole stacking of the layers does not account for the enhanced MO activity in the IFM structure. Certainly, the absolute values of $|Q|$ obtained with the effective medium model in Fig. 5(a) differ from those of the layer-by-layer model in Fig. 5(b). The latter come out to be larger because in the layer-by-layer model all the MO activity is mapped onto only a fraction of the sample, namely, the Fe layers, while in the effective medium model the entirety of the sample is assumed to be magneto-optically active. Notably, $|Q|$ obtained in Fig. 5(b) is much larger than that of bulk Fe ($|Q| = 35 \times 10^{-3}$) at approximately $\lambda = 633$ nm [60,61]. The inset in Fig. 5(b) shows the spectral dependencies of the phase of $|Q|$ for the layer-by-layer model for both samples, which have a behavior similar to that of the curves in the inset of Fig. 5(a). Overall, we consistently observe an enhanced MO activity and enhanced MO coupling Q both with an effective medium model and a layer-by-layer model of the two samples.

E. Analysis with platinum-film-induced additional MO signal

Last but not least, even if one assumes a specific MO interface effect between Fe and Pt layers [62,63], a simple alternative picture of local optical properties cannot consistently explain the results. As compiled in the Supplemental Material [64], we analyze our data by including the possibility of a Pt-film-induced additional MO signal at each surface. To this end, a 2-Å-thick interfacial Pt layer is assumed to have a nonzero Q, while the Pt not at the interface has $Q = 0$. Fe layers are always thin, so no separation between interfacial and "bulk" properties has been considered.

We follow different approaches to try to fit optical models including magneto-optically active interfacial Pt to our experimental data. Figure 6 shows θ_K and η_K for both samples. The red lines in Fig. 6 show the fitting results of the data of the IFM sample with a model that reproduces the
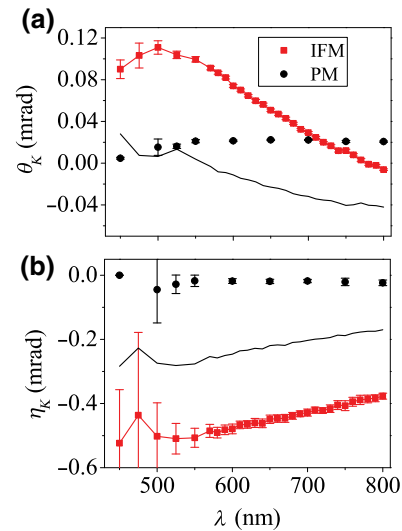

FIG. 6. (a) θ_K and (b) η_K as a function of λ. The symbols represent experimental data points, red squares for the IFM sample and black circles for the PM sample. The red lines in (a),(b) are fits of the IFM sample data considering a structural model that includes magneto-optically active interfacial Pt. The fitting parameters of the model are n, κ, Q_r, and Q_i, which are assumed to be the same for Fe and the interfacial Pt. The black lines in (a) and (b) are θ_K and η_K calculated for an optical model of the PM sample, assuming the n, κ, Q_r, and Q_i fitted for the IFM sample.

structure of IFM, including the interfacial Pt layers. The fitting parameters are the wavelength-dependent n, κ, Q_r, and Q_i of interfacial Pt and Fe, which are considered to be identical. The refractive indices of the rest of the materials are fixed to literature values [57–59]. As it can be observed in Fig. 6, the experimental data are adequately fitted. The fitted n, κ, Q_r, and Q_i of the interfacial Pt and Fe are then utilized to calculate the optical and MO response of a multilayer system reproducing the PM sample, including the interfacial Pt layers. The resulting θ_K and η_K are shown as a solid black line in Figs. 6(a) and 6(b), respectively. As observed, this calculation yields θ_K and η_K that are substantially larger in absolute value than the experimental results. This clearly indicates that just adding a specific MO interface effect between Fe and Pt layers may not be a sufficient explanation for the different results.

In addition, as shown in the Supplemental Material [64], we carry out further trials by fitting the data of both samples simultaneously using four fitting parameters, keeping identical Q and N between Fe and interfacial MO-active Pt; six fitting parameters, keeping identical N between Fe and interfacial MO-active Pt, but different Q; and six fitting parameters, keeping identical Q between Fe and interfacial MO-active Pt, but different N. All trials fail to reproduce the experimental data or to yield sensible Q and/or N values. The conclusion of our analysis is that there is no sensible way to describe/model both types (PM

and IFM) of samples simultaneously by a layer model, in which optical properties coming from their respective local material are just stacked and their classical response solving Maxwell equations and associated boundary conditions is considered. This failure of a local optical model is reflective of the fact that the IFM sample has a far larger MO response than the periodic one, so that this massive discrepancy cannot be explained by the simple stacking leading to more Fe and interface Pt near the surface for this structure. A more significant collective effect must be the origin of the enhanced effective MO signal in the case of the IFM sample. The boundary conditions modulated by the inverse Fibonacci series will change the overall electronic state of the IFM samples and the resulting nonlocal optical response may be most significantly modified.

IV. CONCLUSIONS

In conclusion, utilizing GME in the visible and near-infrared regions, we find that MO parameters, i.e., θ_K, η_K, and Q, for the modulated Fe-Pt IFM metamaterial are far larger than those for a Fe-Pt PM reference sample. The θ_K spectrum is strongly dependent on λ with a sign change at approximately $\lambda = 775$ nm. The η_K remains negative in the explored wavelength region, but shows a 40% decrease in absolute value from $\lambda = 550$ nm to $\lambda = 850$ nm. Since neither Q_r nor Q_i changes sign, the sign change in θ_K is traced back to an interplay between Q_r and Q_i, as well as between those and the optical constants. In contrast, the PM sample shows significantly smaller MO parameters and wavelength dependence. Although the PM and IFM samples containing identical Fe volume show very similar optical constants and in-plane magnetization curves, they exhibit vastly different MO parameters. The IFM sample has a far larger MO response than the periodic one, so that the massive discrepancy cannot be explained by the simple stacking leading to more Fe and interface Pt near the surface for this structure. A more significant collective effect must be the origin of the enhanced effective MO signal in the case of the IFM sample. The present study demonstrates the independent control of the MO and optical parameters, thus opening a door for a new avenue of modulated magnetic metamaterials, such as, for example, for magnetoplasmonic detection to be utilized in biosensing.

[1] H. E. Stanley, *Introduction to Phase Transitions and Critical Phenomena* (Oxford Univ. Press, New York, 1988).

[2] E. N. Economou, *The Physics of Solids: Essentials and Beyond*, Graduate Texts in Physics (Springer, Heidelberg, 2010).

[3] M. Kohmoto, L. P. Kadanoff, and C. Tang, Localization Problem in one Dimension: Mapping and Escape, Phys. Rev. Lett. **50**, 1870 (1983).

[4] R. Merlin, K. Bajema, Roy Clarke, F. Y. Juang, and P. K. Bhattacharya, Quasiperiodic GaAs-AlAs Heterostructures, Phys. Rev. Lett. **55**, 1768 (1985).

[5] D. Shechtman, I. Blech, D. Gratias, and J. W. Cahn, Metallic Phase with Long-range Orientational Order and no Translational Symmetry, Phys. Rev. Lett. **53**, 1951 (1984).

[6] A. Gopinath, S. V. Boriskina, N.-N. Feng, B. M. Reinhard, and L. Dal Negro, Photonic-plasmonic scattering resonances in deterministic aperiodic structures, Nano Lett. **8**, 2423 (2008).

[7] A. Gopinath, S. V. Boriskina, W. R. Premasiri, L. Ziegler, B. M. Reinhard, and L. Dal Negro, Plasmonic nanogalaxies: Multiscale aperiodic arrays for surface-enhanced Raman sensing, Nano Lett. **9**, 3922 (2009).

[8] C. Forestiere, G. Miano, C. Serpico, M. d'Aquino, and L. Dal Negro, Dipolar mode localization and spectral gaps in quasi-periodic arrays of ferromagnetic nanoparticles, Phys. Rev. B **79**, 214419 (2009).

[9] V. S. Bhat, J. Sklenar, B. Farmer, J. Woods, J. T. Hastings, S. J. Lee, J. B. Ketterson, and L. E. De Long, Controlled Magnetic Reversal in Permalloy Films Patterned into Artificial Quasicrystals, Phys. Rev. Lett. **111**, 077201 (2013).

[10] X. Feng, T. Yu, Y. Wei, C. Ji, Y. Cheng, H. Zong, K. Wang, Z. Yang, X. Kang, G. Zhang, and S. Fan, Grouped and multistep nanoheteroepitaxy: Toward high-quality GaN on quasi-periodic nano-mask, ACS Appl. Mater. Interfaces. **8**, 18208 (2016).

[11] Y. Jin, Y. Wang, M. Chen, X. Xiao, T. Zhang, J. Wang, K. Jiang, S. Fan, and Q. Li, Highly sensitive, uniform, and reproducible surface-enhanced Raman spectroscopy substrate with nanometer-scale quasi-periodic nanostructures, ACS Appl. Mater. Interfaces **9**, 32369 (2017).

[12] R. Dhama, V. Caligiuri, L. Petti, A. R. Rashed, M. Rippa, R. Lento, R. Termine, H. Caglayan, and A. De Luca, Extraordinary effects in quasi-periodic gold nanocavities: Enhanced transmission and polarization control of cavity modes, ACS Nano. **12**, 504 (2018).

[13] Y. Moritake, K. Nakayama, T. Suzuki, H. Kurosawa, T. Kodama, S. Tomita, H. Yanagi, and T. Ishihara, Lifetime reduction of a quantum emitter with quasiperiodic metamaterials, Phys. Rev. B **90**, 075146 (2014).

[14] M. S. Vasconcelos, E. L. Albuquerque, and A. M. Mariz, Optical localization in quasi-periodic multilayers, J. Phys.: Condens. Matter. **10**, 5839 (1998).

[15] P. He, W. A. McGahan, J. A. Woollam, F. Sequeda, T. McDaniel, and H. Do, Magneto-optical Kerr effect and

perpendicular magnetic anisotropy of evaporated and sputtered Co/Pt multilayer structures, J. Appl. Phys. **69,** 4021 (1991).

[16] G. Y. Guo and H. Ebert, Band-theoretical investigation of the magneto-optical Kerr effect in Fe and Co multilayers, Phys. Rev. B **51,** 12633 (1995).

[17] S. Uba, L. Uba, A. N. Yaresko, A. Ya. Perlov, V. N. Antonov, and R. Gontarz, Optical and magneto-optical properties of Co/Pt multilayers, Phys. Rev. B **53,** 6526 (1996).

[18] X. Gao, D. W. Glenn, S. Heckens, D. W. Thompson, and J. A. Woollam, Spectroscopic ellipsometry and magneto-optic Kerr effects in Co/Pt multilayers, J. Appl. Phys. **82,** 4525 (1997).

[19] K. Takanashi, S. Mitani, K. Himi, and H. Fujimori, Oscillatory perpendicular magnetic anisotropy and lattice plane spacing in Fe/Au superlattices, Appl. Phys. Lett. **72,** 737 (1998).

[20] F. Iskandar, T. Iwaki, T. Toda, and K. Okuyama, High coercivity of ordered macroporous FePt films synthesized via colloidal templates, Nano Lett. **5,** 1525 (2005).

[21] T. Katayama, H. Awano, and Y. Nishihara, Wavelength dependence of magneto-optical Kerr rotation in Co/Cu, Fe/Cu, Co/Au and Fe/Au compositionally modulated multilayered films, J. Phys. Soc. Jpn. **55,** 2539 (1986).

[22] W. B. Zeper, F. J. A. M. Greidanus, P. F. Carcia, and C. R. Fincher, Perpendicular magnetic anisotropy and magneto-optical Kerr effect of vapor-deposited Co/Pt-layered structures, J. Appl. Phys. **65,** 4971 (1989).

[23] K. Sato, H. Hongu, H. Ikekame, J. Watanabe, K. Tsuzukiyama, Y. Togami, M. Fujisawa, and T. Fukazawa, Magnetooptical spectra in Pt/Co and Pt/Fe multilayers, Jpn. J. Appl. Phys. **31,** 3603 (1992).

[24] S. Mitani, K. Takanashi, M. Sano, H. Fujimori, A. Osawa, and H. Nakajima, Perpendicular magnetic anisotropy and magneto-optical Kerr rotation in FePt(001) monoatomic multilayers, J. Magn. Magn. Mater. **148,** 163 (1995).

[25] K. Takanashi, S. Mitani, H. Fujimori, K. Sato, and Y. Suzuki, Magnetooptical Kerr effect in Fe/Au superlattices modulated by integer atomic layers, J. Magn. Magn. Mater. **177-181,** 1199 (1998).

[26] T.-S. Liu and G.-Z. Wei, Spin waves in quasiperiodic layered ferromagnets, Phys. Rev. B **48,** 7154 (1993).

[27] D. H. A. L. Anselmo, M. G. Cottam, and E. L. Albuquerque, Magnetostatic modes in quasiperiodic Fibonacci magnetic superlattices, J. Appl. Phys. **85,** 5774 (1999).

[28] C. H. Costa and M. S. Vasconcelos, Magnons in one-dimensional k-component Fibonacci structures, J. Appl. Phys. **115,** 17C115 (2014).

[29] J. Rychły, J. W. Kłos, M. Mruczkiewicz, and M. Krawczyk, Spin waves in one-dimensional bicomponent magnonic quasicrystals, Phys. Rev. B **92,** 054414 (2015).

[30] L. D. Machado, C. G. Bezerra, M. A. Correa, C. Chesman, J. E. Pearson, and A. Hoffmann, Anomalous magnetoresistance in Fibonacci multilayers, Phys. Rev. B **85,** 224416 (2012).

[31] L. D. Machado, C. G. Bezerra, M. A. Correa, C. Chesman, J. E. Pearson, and A. Hoffmann, Static and dynamic properties of Fibonacci multilayers, J. Appl. Phys. **113,** 17C102 (2013).

[32] T. Suwa, S. Tomita, N. Hosoito, and H. Yanagi, Magnetic properties of Fibonacci-modulated Fe-Au multilayer metamaterials, Materials **10,** 1209 (2017).

[33] A. Berger and M. R. Pufall, Generalized magneto-optical ellipsometry, Appl. Phys. Lett. **71,** 965 (1997).

[34] A. Berger and M. R. Pufall, Quantitative vector magnetometry using generalized magneto-optical ellipsometry, J. Appl. Phys. **85,** 4583 (1999).

[35] D. Schmidt, T. Hofmann, C. M. Herzinger, E. Schubert, and M. Schubert, Magneto-optical properties of cobalt slanted columnar thin films, Appl. Phys. Lett. **96,** 091906 (2010).

[36] K. Mok, N. Du, and H. Schmidt, Vector-magneto-optical generalized ellipsometry, Rev. Sci. Instrum. **82,** 033112 (2011).

[37] J. A. Arregi, J. B. Gonzalez-Diaz, E. Bergaretxe, O. Idigoras, T. Unsal, and A. Berger, Study of generalized magneto-optical ellipsometry measurement reliability, J. Appl. Phys. **111,** 103912 (2012).

[38] C. Briley, D. Schmidt, T. Hofmann, E. Schubert, and M. Schubert, Anisotropic magneto-optical hysteresis of permalloy slanted columnar thin films determined by vector magneto-optical generalized ellipsometry, Appl. Phys. Lett. **106,** 133104 (2015).

[39] P. Riego, S. Vélez, J. M. Gomez-Perez, J. A. Arregi, L. E. Hueso, F. Casanova, and A. Berger, Absence of detectable current-induced magneto-optical Kerr effects in Pt, Ta, and W, Appl. Phys. Lett. **109,** 172402 (2016).

[40] G. Neuber, R. Rauer, J. Kunze, T. Korn, C. Pels, G. Meier, U. Merkt, J. Bäckström, and M. Rübhausen, Temperature-dependent spectral generalized magneto-optical ellipsometry, Appl. Phys. Lett. **83,** 4509 (2003).

[41] K. Mok, G. J. Kovács, J. McCord, L. Li, M. Helm, and H. Schmidt, Magneto-optical coupling in ferromagnetic thin films investigated by vector-magneto-optical generalized ellipsometry, Phys. Rev. B **84,** 094413 (2011).

[42] P. Riego, S. Tomita, K. Murakami, T. Kodama, N. Hosoito, H. Yanagi, and A. Berger, Enhanced magneto-optical Kerr effects in Py/Ag/Bi trilayers, J. Phys. D: Appl. Phys. **50,** 19LT01 (2017).

[43] J. B. Pendry, A. J. Holden, W. J. Stewart, and I. Youngs, Extremely Low Frequency Plasmons in Metallic Mesostructures, Phys. Rev. Lett. **76,** 4773 (1996).

[44] J. B. Pendry, A. J. Holden, D. J. Robbins, and W. J. Stewart, Magnetism from conductors and enhanced nonlinear phenomena, IEEE Trans. Microw. Theory. Tech. **47,** 2075 (1999).

[45] D. R. Smith, D. C. Vier, Willie Padilla, Syrus C. Nemat-Nasser, and S. Schultz, Loop-wire medium for investigating plasmons at microwave frequencies, Appl. Phys. Lett. **75,** 1425 (1999).

[46] D. R. Smith, W. J. Padilla, D. C. Vier, S. C. Nemat-Nasser, and S. Schultz, Composite Medium with Simultaneously Negative Permeability and Permittivity, Phys. Rev. Lett. **84,** 4184 (2000).

[47] S. Tomita, K. Sawada, A. Porokhnyuk, and T. Ueda, Direct Observation of Magnetochiral Effects through a Single Metamolecule in Microwave Regions, Phys. Rev. Lett. **113,** 235501 (2014).

[48] S. Tomita, H. Kurosawa, T. Ueda, and K. Sawada, Metamaterials with magnetism and chirality, J. Phys. D: Appl. Phys. **51**, 083001 (2018).

[49] D. R. Smith, J. B. Pendry, and M. C. K. Wiltshire, Metamaterials and negative refractive index, Science **305**, 788 (2004).

[50] N. Maccaferri, K. E. Gregorczyk, T. V. A. G. de Oliveira, M. Kataja, S. van Dijken, Z. Pirzadeh, A Dmitriev, J. Åkerman, M. Knez, and P. Vavassori, Ultrasensitive and label-free molecular-level detection enabled by light phase control in magnetoplasmonic nanoantennas, Nat. Commun. **6**, 6150 (2015).

[51] J. Yang, M. Donolato, A. Pinto, F. G. Bosco, E.-T. Hwu, C.-H. Chen, T. S. Alstrøm, G.-H. Lee, T. Schafer, P. Vavassori, A. Boisen, Q. Lin, and M. F. Hansen, Blu-ray based optomagnetic aptasensor for detection of small molecules, Biosens. Bioelectron. **75**, 396 (2016).

[52] M. Kataja, S. Pourjamal, N. Maccaferri, P. Vavassori, T. K. Hakala, M. J. Huttunen, P. Törmä, and S. van Dijken, Hybrid plasmonic lattices with tunable magneto-optical activity, Opt. Express **24**, 3652 (2016).

[53] N. Maccaferri, L. Bergamini, M. Pancaldi, M. K. Schmidt, M. Kataja, S. van Dijken, N. Zabala, J. Aizpurua, and P. Vavassori, Anisotropic nanoantenna-based magnetoplasmonic crystals for highly enhanced and tunable magneto-optical activity, Nano Lett. **16**, 2533 (2016).

[54] E. Goering, J. Will, J. Geissler, M. Justen, F. Weigand, and G. Schuetz, X-ray magnetic circular dichroism − a universal tool for magnetic investigations, J. Alloys. Compd. **328**, 14 (2001).

[55] M. Suzuki, H. Muraoka, Y. Inaba, H. Miyagawa, N. Kawamura, T. Shimatsu, H. Maruyama, N. Ishimatsu, Y. Isohama, and Y. Sonobe, Depth profile of spin and orbital magnetic moments in a subnanometer Pt film on Co, Phys. Rev. B **72**, 054430 (2005).

[56] M. Schubert, Polarization-dependent optical parameters of arbitrarily anisotropic homogeneous layered systems, Phys. Rev. B **53**, 4265 (1996).

[57] W. S. M. Werner, K. Glantschnig, and C. Ambrosch-Draxl, Optical constants and inelastic electron-scattering data for 17 elemental metals, J. Phys. Chem. Ref. Data **38**, 1013 (2009).

[58] P. B. Johnson and R. W. Christy, Optical constants of transition metals: Ti, V, Cr, Mn, Fe, Co, Ni, and Pd, Phys. Rev. B **9**, 5056 (1974).

[59] R. E. Stephens and I. H. Malitson, Index of refraction of magnesium oxide, J. Res. Natl. Bur. Stand. **49**, 249 (1952).

[60] C. C. Robinson, Longitudinal Kerr magneto-optic effect in thin films of iron, nickel, and permalloy, J. Opt. Soc. Am. **53**, 681 (1963).

[61] G. A. Prinz, J. J. Krebs, D. W. Forester, and W. G. Maisch, Magneto-optical characterization of Fe and Co-based alloy films, J. Magn. Magn. Mater. **15-18**, 779 (1980).

[62] X. Gao, D. W. Thompson, and J. A. Woollam, Determination of the interfacial magneto-optical effects in Co/Pt multilayer structures, Appl. Phys. Lett. **70**, 3203 (1997).

[63] X. Gao, M. J. DeVries, D. W. Thompson, and J. A. Woollam, Thickness dependence of interfacial magneto-optic effects in Pt/Co multilayers, J. Appl. Phys. **83**, 6747 (1998).

[64] See the Supplemental Material at http://link.aps.org/supplemental/10.1103/PhysRevApplied.11.064010 for analysis with the possibility of a Pt-film-induced additional MO signal at each surface.